Ore Geology Reviews 91 (2017) 100–109

Contents lists available at ScienceDirect

Ore Geology Reviews

journal homepage: www.elsevier.com/locate/oregeorev

REE mineralization in the Bayan Obo deposit, China: Evidence from mineral paragenesis

Miao Deng[a], Cheng Xu[a,*], Wenlei Song[a], Haiyan Tang[b], Yun Liu[b], Qiang Zhang[b], Yue Zhou[b], Meng Feng[a], Chunwan Wei[a]

[a] Laboratory of Orogenic Belts and Crustal Evolution, School of Earth and Space Sciences, Peking University, Beijing 100871, China
[b] Exploration and Survey Institute of Baogang Group, Baotou 014010, China

ARTICLE INFO

Keywords:
Bayan Obo
Rare earth elements
Apatite
Monazite
Multi-stage metasomatism

ABSTRACT

Preliminary mineralogical and geochemical studies have been carried out on dolomite marble drill cores from the Bayan Obo REE deposit in China. Three types of apatites and four types of monazites have been identified based on textural features: Type 1 apatite occurs as grains with minor monazite (Type 1 monazite) on its border; Type 2 apatite veinlet shows clusters of assemblages with abundant bastnäsite and parisite at the rim; Type 3 apatite has a linear array associated with fluorite and bastnäsite veinlets. Type 2 monazite occurs as clusters intergrowing with parisite and fluorite. Type 3 and 4 monazites occur as polymineralic (fluorite and bastnäsite) and monomineralic veinlets, respectively. These four types of monazites have similar LREE composition but variable Y content (Y_2O_3 ranging from below determination limits to 0.7 wt%). The three types of apatites also show different REE content and distribution patterns, ranging from high REE abundance (ΣREE + Y: 27243–251789 ppm) and strong LREE enrichment [$(La/Yb)_{CN}$ ~101] in Type 1, less LREE enrichment [$(La/Yb)_{CN}$ ~8] in Type 2 to relatively low REE abundance (ΣREE + Y: 4323–11175 ppm) but high REE fractionation [$(La/Yb)_{CN}$ ~58] in Type 3. The primary apatite has high Sr (5461–6892 ppm) and REE content, implying a carbonatite origin. The late-stage apatites (Types 2 and 3) show different Sr and REE abundances. Significant differences in their Sr composition (6189 ± 573, 6041 ± 549 and 3492 ± 802 for Types 1–3 samples, respectively) and Y/Ho ratio (20.9 ± 0.11, 19.5 ± 0.17 and 17.4 ± 0.37, respectively) indicate that the three types of apatites may have crystallized from different metasomatic fluids. Multi-stage metasomatism resulted in remobilization and redeposition of primary REE minerals to form the Bayan Obo REE deposit.

1. Introduction

Rare earth elements (REE) are important for high-technology industries. China supplies about 83% of the world's REE, but has decided to reduce REE exports because of environment issues (Liu and Hou, 2017; U.S. Geological Survey, 2017). As a consequence, there is an increasing interest in exploring for new sources of these elements worldwide. The Bayan Obo deposit is the world's largest REE deposit and it has attracted intense scientific study. However, the origin of the deposit remains a subject of great debate. Various models have been proposed, including large-scale carbonatite magmatism (Yang and Le Bas, 2004; Xu et al., 2008), metasomatic alteration of a sedimentary marble by hydrothermal fluids (Meng, 1982; Chao et al., 1992), granitic fluids (Wang et al., 1994; Chao et al., 1997), carbonatitic fluids (Smith et al., 1999; Yang et al., 2009, 2017), or Caledonian 'subduction-related' fluids (Ling et al., 2013). A number of studies clearly show that the deposit underwent stages of hydrothermal activity and metasomatic alteration (Chao et al., 1997; Ling et al., 2013; Smith et al., 2015). Different ore types have been recognized, and were overprinted by many hydrothermal minerals such as fluorite, aegirine, riebeckite and mica. Owing to the overprinting of hydrothermal processes (Smith et al., 2015), the textural and temporal relations between the primary minerals and alteration assemblages complicates the interpretation of REE mineralization. Therefore, an attempt to trace the origin of the primary REE mineralization is extremely difficult. In this study we obtained drill core samples from 223 m to 1775 m. Their ore mineralogy and paragenesis are relatively less complicated relative to those of surface samples with strong alteration. We report different textures of monazites and apatites, in order to offer new clues for restricting the source of ore-forming fluids and tracing the origin of REE mineralization.

* Corresponding author.
E-mail address: xucheng1999@pku.edu.cn (C. Xu).

http://dx.doi.org/10.1016/j.oregeorev.2017.10.018
Received 20 June 2017; Received in revised form 15 October 2017; Accepted 20 October 2017
Available online 21 October 2017

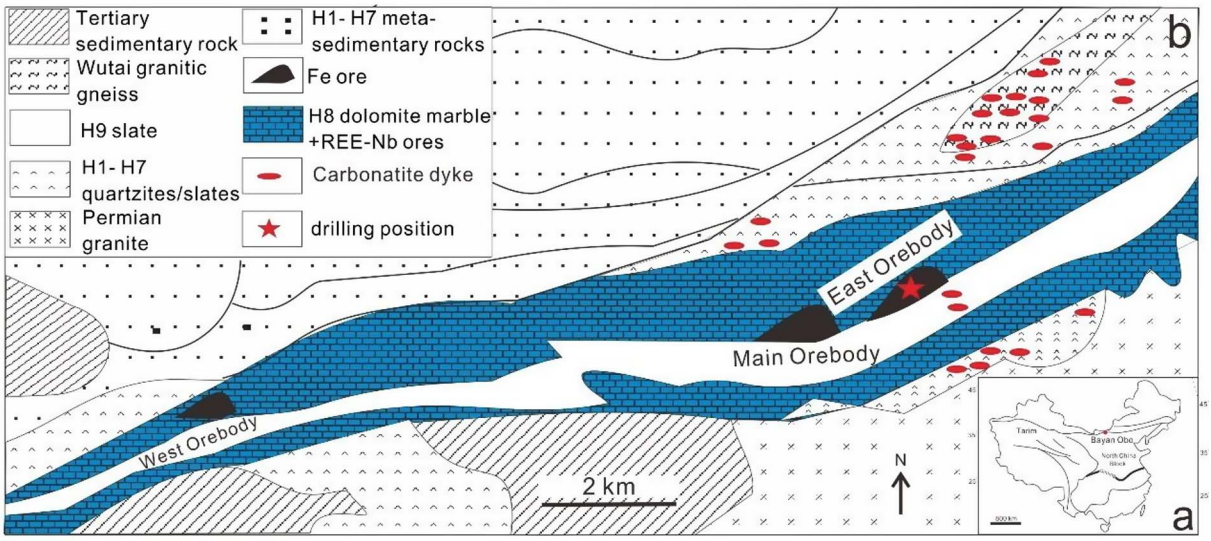

Fig. 1. Geological sketch of the Bayan Obo REE deposits. Modified from Xu et al. (2008).

2. Geological setting and sampling

2.1. Geological background

The Bayan Obo deposit is situated on the northern margin of the North China Craton (109°59′E; 41°48′N), which was formed through accretion of microcontinental blocks from 2.2 to 1.85 Ga (Zhao et al., 2003). In the Mesoproterozoic period the northern part of the craton underwent rifting (Yang et al., 2009; Zhao et al., 2003), resulting in the formation of numerous carbonatite dykes close to the deposit (~1.3 Ga: Yang et al., 2011; Fan et al., 2014; Zhang et al., 2017). The basement in this region is composed of the Proterozoic Bayan Obo and Wutai groups (gneisses and migmatites), which significantly pre-dates mineralization of the deposit (Chao et al., 1997). The Bayan Obo group has been subdivided into nine lithological units, H1–H9 in ascending order (Bai and Yuan, 1985). It predominantly consists of meta-sandstones and slates, with the exception of the H8 dolomite marble. The giant REE deposit is hosted in the H8 dolomite marble, and is overlain by the schist, black shale and slate of the H9 unit. This ore-hosting H8 unit extends 18 km from west to east, with a width of more than 1 km and occurs as a spindle-shaped stratiform body (Fig. 1). The H8 unit has massive and banded structures with coarse- and fine-grained textures, and is mostly composed of dolomite and calcite, with minor feldspar, magnesio-arfvedsonite, phlogopite, Na-tremolite, quartz, barite, fluorite, apatite, sulfide, and REE minerals. The origins of the dolomite marble are disputed and interpretations include sedimentary formation or carbonatite magmatism (Xu et al., 2008). The Bayan Obo deposit is the world's largest REE deposit with reserves estimated to be more than 120 Mt REE_2O_3 (Xie et al., 2016).

REE ores occur throughout the entire H8 dolomite marble. According to the characteristic mineral associations (> 10%; Institute of Geochemistry, Chinese Academy of Sciences, 1988), the ore bodies can be divided into nine groups (Table 1), and REE ores occur as massive, banded and disseminated, with disseminated dolomite-REE ore being the main type. The wide distribution of fenitization and alteration within the H8 dolomite marble produces different mineral assemblages of fluorite, aegirine, arfvedsonite, phlogopite and diopside, forming different ore types. The textures and compositions of the metasomatic silicate minerals in the ore bodies, as reported by Smith (2007), indicate a multistage fluid evolution history. Fluorite is a typical gangue mineral and is presented in all ore bodies with general 1–10% volume and trace amounts in the diopside-phlogopite-REE ore (Xu et al., 2012).

The drill cores were collected in the eastern ore bodies from depths of 223 to 1775 m. The samples are composed of coarse- and fined-grained dolomite marbles (Fig. 2). The coarse-grained dolomite marble mainly consists of euhedral to subhedral dolomite with a diameter of more than 0.5 mm, which shows a lineation structure resulting from deformation events. These coarse-grained dolomites have clearly defined triple junctions. The fine-grained dolomite marble is composed of dolomite and ankerite less than 0.5 mm in diameter. The REE mineral paragenesis of the H8 marble is complex, and almost all the reported REE minerals have been associated with metasomatic silicate minerals of aegirine, riebeckite, and late-stage barite and fluorite veinlets. Similar mineral occurrences were found in our drill core samples. Note that independent REE mineralization has been identified in this study.

2.2. Sampling

Monazite, REE-fluorocarbonates and apatite are representative REE minerals in Bayan Obo. The paragenesis of REE minerals in the surface samples is extremely complex. Smith et al. (1999) summarized five stages: disseminated monazite, banded ores, and aegirine, fluorite, barite veins. In disseminated ores, monazite concentrated along fractures and grain boundaries in the dolomite marble. In the banded ores, monazite, bastnäsite and apatite occurred in bands, and were followed by the widespread replacement of aegirine-augite and fluorite. The banded ore was cut by aegirine, fluorite and barite veins, in which REE-fluorocarbonate mineralisation developed. In contrast, the relative paragenesis of main REE minerals in the drill cores is simple. Based on textural features, three types of apatites and four types of monazites can be identified.

2.2.1. Apatite

The apatite shows variable sizes, ranging from coarse (up to 0.2 mm) to fine (< 10 μm) grains. Type 1 apatite occurs as grains with minor monazites on its border (Fig. 3a). Type 2 apatite displays a prominent lineation, with bastnäsite and parisite intergrowing around apatites (Fig. 3b). The REE minerals may be produced by dissolution and reprecipitation of the apatite. Type 3 apatite shows disseminated texture (Fig. 3c, d) and it mostly shows a linear array associated with fluorite and bastnäsite-parisite veinlets. The apatite crystallized simultaneously with the REE minerals. The variations in apatite have previously been reported by Campbell and Henderson (1997), who identified apatite textures including massive aggregates and vein associated with fluorite.

Table 1
Reported REE ore types in the Bayan Obo deposit.

Ore types*	Distribution	Composition of minerals	
		> 10% Minerals	1–10% Minerals
Massive Nb-REE-Fe ore	Main and eastern ore bodies	Magnetite, fluorite	Aegirine, riebeckite, phlogopite, monazite, bastnäsite, hematite
Banded Nb-REE-Fe ore	Main and eastern ore bodies	Fluorite, hematite, bastnäsite	Magnetite, barite, dolomite, apatite, quartz, monazite
Aegirine-type Nb-REE-Fe ore	Main and eastern ore bodies	Aegirine, magnetite	Monazite, bastnäsite, barite, fluorite, quartz, apatite, hematite
Riebeckite-type Nb-REE-Fe ore	Main, western and eastern ore bodies	Riebeckite, magnetite, phlogopite, muscovite	Monazite, fluorite, bastnäsite, pyrite
Biotite-type Nb-REE-Fe ore	Main, eastern and western ore bodies	Biotite, magnetite	Riebeckite, phlogopite, fluorite, feldspar
Dolomite-type Nb-REE-Fe ore	Western and main ore bodies	Dolomite, magnetite	Riebeckite, phlogopite, fluorite, barite, apatite, monazite
Aegirine-type Nb-REE ore	Main and eastern ore bodies	Aegirine	Fluorite, bastnäsite, monazite, barite, riebeckite, magnetite, apatite, quartz, cordylite
Dolomite-type Nb-REE ore	main eastern and western ore bodies	Dolomite	Monazite, magnetite, riebeckite, phlogopite, fluorite

*Institute of Geochemistry, Chinese Academy of Sciences (1988).

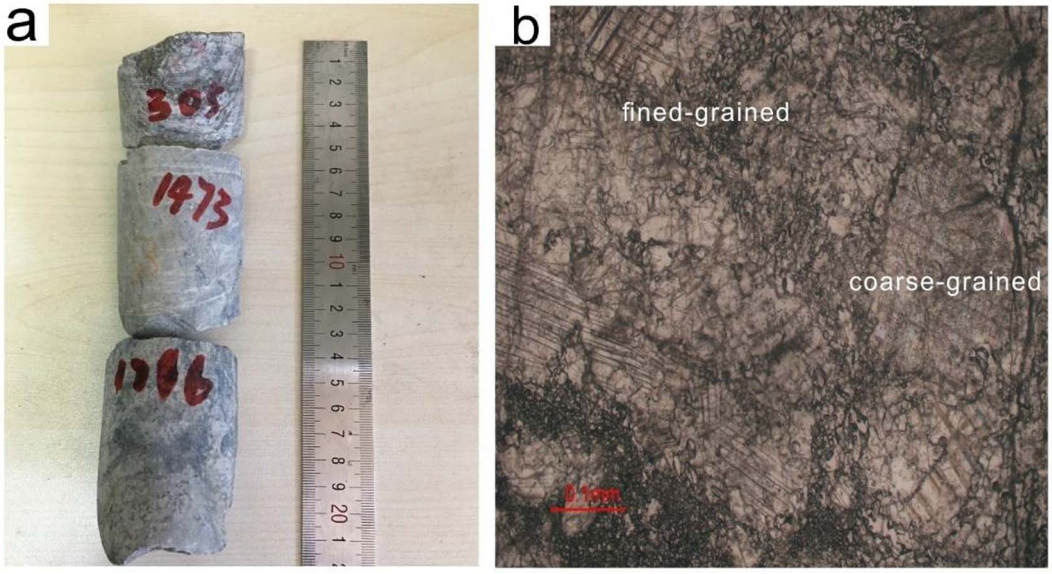

Fig. 2. Photographs of representative drill core samples (a) and coarse-grained, fined-grained dolomite marble under cross-polarized light (b).

2.2.2. Monazite

Type 1 monazite shows overgrowth texture within the precursor apatite (Fig. 4a). Type 2 monazite is disseminated and occurs as clusters intergrowing with parisites and flourites (Fig. 4b, c). Type 3 monazite occurs as veinlets displaying lineation parallel with fluorite and bastnäsite veinlets (Fig. 4d, e). Type 4 monazite occurs as monomineralic veinlets (Fig. 4f), without the presence of fluorite or other REE minerals. This type of monazite has not been observed in previous publications. There is limited data available on the distinct textural and chemical features of monazites in the Bayan Obo deposit. The reported monazites are generally associated with metasomatic silicate minerals of aegirine, riebeckites, and flourites (Wang et al., 1994; Smith et al., 1999).

3. Analytical methods

Major-element compositions of REE minerals in the drill cores were determined by wavelength-dispersive X-ray spectrometry (WDS) using a JEOL JXA-8230 electron microprobe at the Guilin University of Technology, China. The microprobe was operated at an accelerating voltage of 20 kV and a beam current of 20 nA, with an electron beam defocused to a 5–10-μm spot to limit ionic diffusion, devolatilisation and other forms of beam damage in the samples. For the analysed minerals, their own set of appropriate matrix-specific standards (both natural and synthetic) and optimal instrumental conditions (beam settings, detector type and counting statistics) were carefully chosen by performing multiple measurements. The following standards and crystals were used in the analysis: jadetite, Si, Al, Na; forsterite, Mg; topaz, F; K-feldspar, K; wollastonite, Ca; hematite, Fe; apatite, P; MnO, Mn; celestine, Sr; NaCl, Cl. For REE minerals, raw WDS data were corrected using empirical interference values for REE and other elements potentially interfering with the REE signals determined for the well-characterised synthetic standards (glasses and orthophosphates). The data were reduced using the PAP routine. Analytical precision for the most of the elements analyzed is better than 0.1% relative to oxides. In-situ laser-ablation ICPMS at Peking University was used to measure the abundances of selected trace elements in the apatites of representative polished thin sections. The diameter of the ablation spot ranged between 40 μm depending on the size and compositional homogeneity of individual mineral grains. The NIST610 glass was used for external calibration. The Ca content determined independently by WDS was used as an internal standard. The analytical precision is estimated to be better than 5% at the ppm level.

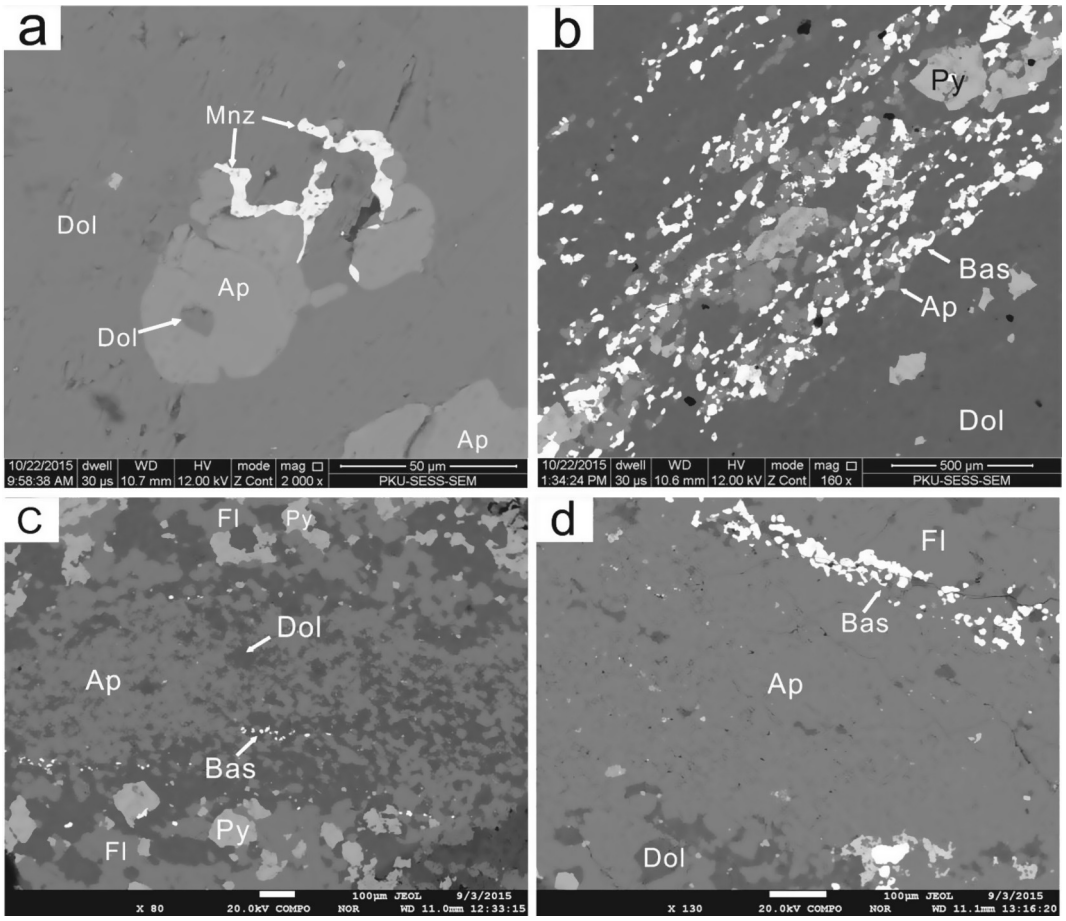

Fig. 3. Backscattered electron images of three types of apatite. (a) Type 1, primary grain altered to form minor monazite; (b) Type 2, veinlets intergrowing with bastnäsite grains; (c) (d) Type 3, disseminated texture and a linear array associated with fluorite veinlet. Abbreviations: Dol, dolomite; Mnz, monazite; Bas, bastnäsite; Fl, fluorite; Py, pyrite.

4. Results

4.1. Dolomite

The carbonate minerals are characterized by higher Fe, Ca but lower Mg contents (6.7–9.7 wt% FeO; 30–31 wt% CaO; 14–18 wt% MgO) (Table 2), and show coarse- and fine-grained textures. No obviously compositional difference in major elements was observed. Both the fine- and coarse-grained dolomites contain high SrO abundance (0.05–0.15 wt% and 0.1–0.18 wt%, respectively), similar to carbonatitic carbonate minerals (Chakhmouradian et al., 2016).

4.2. Apatite

Apatite contains a high level of F (2.0–4.4 wt%) and belongs to fluorapatite (Table 2). The three types of apatites show different REE content and distribution patterns (Fig. 5a). Type 1 apatite, occurring as euhedral grains, is characterized by the highest REE abundance (La: 1461–11641 ppm) (Table 3) and strongest LREE enrichment [$(La/Yb)_{CN}$ = 30–291]. These results are similar to the apatite from the carbonatite dykes near to the deposit, as described by Le Bas et al. (1992). Type 2 apatite occurs in clusters of assemblages associated with abundant monazite and bastnäsite grains, and exhibits less LREE enrichment [$(La/Yb)_{CN}$ = 5–11], but its HREE content is similar to Type 1 sample. Type 3 apatite shows disseminated texture, with a linear array associated with fluorite veinlets. It contains lower REE abundance (La: 447–1419 ppm), but has a LREE enrichment pattern [$(La/Yb)_{CN}$ = 39–83] similar to Type 1 apatite. Note that the three types of apatites contain high Sr content (5461–6892 ppm, 4858–6733 ppm and 2228–4368 ppm for Types 1–3 samples, respectively) and do not show obvious Ce and Eu anomalies. In contrast, reported apatites from Campbell and Henderson (1997), analyzed by microprobe and occurring as massive aggregates and association with fluorite vein, contained lower REE abundance (e.g. 0.07–0.36 wt% La_2O_3).

4.3. Monazite

The variation in REE abundance of monazite from the four types is shown in Table 2 and Fig. 5b. The discussion here is limited to the elements in the range La-Dy as some HREE were below detection limits. The four types of monazites have similar LREE abundance and patterns [$(La/Nd)_{CN}$ = 2.1–5.3], but show differences in their Y contents. Type 3, 4 monazites, occurring as veinlets, contain lower Y_2O_3 abundance (~0.04 wt% and ~0.08 wt%, respectively) than Type 1 (~0.38 wt%) and Type 2 (~0.43 wt%) samples. Minor monazites associated with metasomatic silicate minerals and fluorite, observed by Smith et al. (2000), contain similar LREE but higher HREE contents than our samples (Fig. 5b).

5. Discussion

It is well known that the Bayan Obo region underwent metasomatic and metamorphic events (Wang et al., 1994; Chao et al., 1997; Smith et al., 2015). There is a ~1 Ga range in radiometric age determinations for the deposit (see recent articles by Smith et al., 2015; Fan et al., 2016 and Yang et al., 2017). The H8 dolomite marble has a Sm-Nd isochron age of 1.3 Ga (Zhang et al., 2003; Zhu et al., 2015), similar to the carbonatite dykes close to the deposit (whole rock Sm-Nd isochron age:

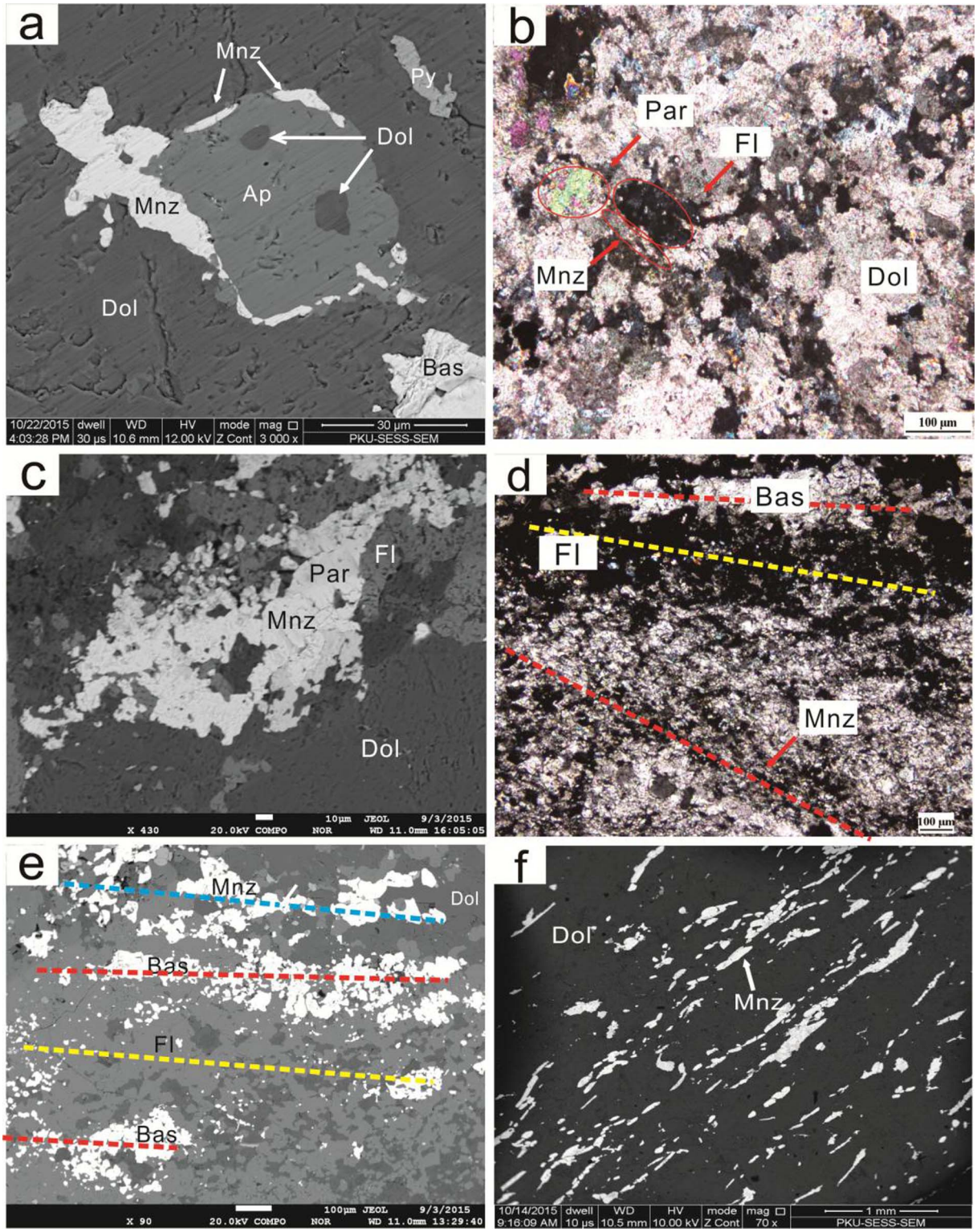

Fig. 4. Backscattered electron (a, b, d, f) and crossed-polarized light (c, e) images of four types of monazites. (a) Type 1, overgrowth texture within the apatite. (b) (c) Type 2, disseminated clusters intergrowing with parisite and fluorite. (d)(e) Type 3, veinlet associated with bastnäsite and fluorite. (e) Type 4, monomineral veinlet. Abbreviations are the same as in Fig. 3.

Yang et al., 2011; Fan et al., 2014; and zircon U-Pb age: Zhang et al., 2017). However, Wang et al. (1994) obtained Th-Pb isochron ages for monazite from the H8 orebody ranging from 555 to 398 Ma. Older monazite ages (ca. 750 Ma) have been reported by Ling et al. (2013). Besides monazite, Sm-Nd dating of huanghoite minerals (Hu et al., 2009) and Re-Os dating of pyrites (Liu, 2004), yield ages between 400 Ma and 500 Ma.

Chao et al. (1997) suggested that there were at least 11 main paragenetic stages, from deposition of the host rocks, through metamorphism and mineralization to the intrusion of Hercynian granitoid south of the deposit. The wide distribution of fenitization and alteration within the H8 marble produced different mineral assemblages of

Table 2
Main element compositions (wt.%) of dolomite, apatite and monazite from drill core samples in the Bayan Obo deposit.

	Coarse-grained dolomite										
Sample	1	2	3	4	5	6	7	8	9	10	11
CaO	30.40	30.70	30.80	30.80	30.60	30.90	30.50	30.80	30.90	31.00	30.10
BaO	0.03	0.03	0.03	0.00	0.00	0.06	0.05	0.01	0.00	0.06	0.00
SrO	0.13	0.14	0.15	0.18	0.17	0.12	0.17	0.12	0.14	0.15	0.10
Na_2O	0.03	0.03	0.08	0.00	0.00	0.00	0.02	0.05	0.01	0.02	0.07
MnO	1.46	1.50	1.46	1.50	1.53	1.57	1.69	1.48	2.08	1.39	1.95
FeO	9.49	9.68	9.65	9.63	9.63	9.43	9.38	9.58	8.27	9.26	9.17
MgO	15.20	14.90	15.00	15.10	15.20	14.90	14.90	15.40	15.70	15.00	14.80
Total	56.80	56.90	57.10	57.20	57.10	57.00	56.70	57.50	57.00	56.90	56.10
	Fine-grained dolomite										
Sample	1	2	3	4	5	6	7	8	9	10	11
CaO	30.80	30.60	30.30	30.40	30.30	30.30	31.10	30.90	30.40	30.50	30.40
BaO	0.04	0.00	0.05	0.03	0.10	0.00	0.07	0.00	0.00	0.00	0.05
SrO	0.11	0.09	0.11	0.07	0.06	0.10	0.16	0.14	0.05	0.13	0.16
Na2O	0.01	0.04	0.04	0.00	0.04	0.06	0.01	0.00	0.05	0.00	0.00
MnO	1.61	3.19	1.72	1.56	1.71	1.78	1.65	1.52	2.34	1.60	3.10
FeO	9.39	6.71	7.49	7.66	7.71	7.82	9.12	9.20	9.21	9.25	7.82
MgO	15.60	16.20	16.90	15.90	17.60	15.90	16.20	16.10	16.00	13.70	14.90
Total	57.60	56.90	56.60	55.60	57.50	56.00	58.30	57.90	58.00	55.20	56.40

	Type 1 apatite																		
Sample	1	2	3	4	5	6	7	8	9	10	11	12	13	14	15	16	17	18	19
F	1.64	3.15	4.41	3.47	3.84	2.81	3.59	2.94	2.23	2.17	2.86	3.25	4.35	4.41	3.52	4.11	3.95	3.28	2.95
Cl	0.01	0.00	0.01	0.01	0.00	0.00	0.00	0.01	0.01	0.01	0.02	0.00	0.00	0.00	0.01	0.01	0.00	0.02	0.01
MnO	0.02	0.04	0.03	0.02	0.04	0.03	0.08	0.08	0.10	0.10	0.03	0.04	0.05	0.07	0.00	0.09	0.05	0.00	0.05
SiO_2	0.02	0.01	0.00	0.03	0.01	0.00	0.02	0.04	0.02	0.01	0.01	0.00	0.01	0.00	0.00	0.02	0.00	0.00	0.01
SrO	0.46	0.42	0.47	0.28	0.24	0.50	0.57	0.43	0.22	0.86	0.25	0.33	0.33	0.31	0.19	0.20	0.14	0.22	0.21
CaO	52.91	53.16	53.22	53.79	53.36	54.48	53.70	53.18	54.37	52.84	54.33	53.84	54.00	53.10	51.94	53.29	53.08	53.38	53.37
P_2O_5	45.01	43.66	42.63	44.18	43.13	42.25	42.33	42.84	43.30	42.76	42.45	42.25	41.97	42.30	42.27	42.46	42.41	39.96	42.38
O = F,Cl	−0.69	−1.33	−1.86	−1.46	−1.62	−1.18	−1.51	−1.24	−0.94	−0.92	−1.21	−1.37	−1.83	−1.86	−1.48	−1.73	−1.66	−1.39	−1.24
Total	99.06	98.21	97.63	99.13	97.68	98.02	97.70	97.47	98.63	97.03	98.70	97.80	97.76	97.10	96.14	97.50	96.71	94.85	96.93
	Type 2 apatite																		
Sample	1	2	3	4	5	6	7	8	9	10	11	12	13	14	15	16			
F	4.02	2.76	3.63	2.87	4.94	2.75	2.66	2.92	3.55	2.84	2.97	3.24	2.59	3.72	3.81	3.90			
Cl	0.01	0.01	0.00	0.00	0.01	0.00	0.00	0.00	0.00	0.00	0.01	0.00	0.01	0.00	0.00	0.00			
MnO	0.06	0.05	0.00	0.02	0.01	0.04	0.01	0.03	0.00	0.00	0.06	0.02	0.04	0.03	0.07	0.08			
SiO_2	0.01	0.00	0.00	0.01	0.00	0.00	0.02	0.00	0.00	0.00	0.01	0.01	0.00	0.00	0.00	0.01			
SrO	0.29	0.37	0.27	0.32	0.43	0.11	0.33	0.37	0.31	0.33	0.14	0.47	0.58	0.54	0.31	0.31			
CaO	53.87	52.89	53.96	52.82	53.74	54.43	52.45	51.02	53.71	53.67	54.36	51.29	52.20	51.79	52.77	53.03			
P_2O_5	43.23	41.50	42.52	42.17	42.41	43.10	45.18	41.48	41.86	42.53	43.00	42.43	42.33	42.12	44.32	41.90			
O = F,Cl	−1.69	−1.16	−1.53	−1.21	−2.08	−1.16	−1.12	−1.23	−1.49	−1.20	−1.25	−1.36	−1.09	−1.57	−1.60	−1.64			
Total	98.52	95.98	97.79	96.67	98.32	98.25	100.93	95.93	96.92	97.37	98.16	95.96	95.96	95.54	98.61	96.24			
	Type 3 apatite																		
Sample	1	2	3	4	5	6	7	8	9										
F	3.24	3.52	2.65	3.07	3.81	4.02	3.25	1.73	3.85										
Cl	0.00	0.01	0.00	0.00	0.00	0.01	0.00	0.00	0.00										
MnO	0.07	0.06	0.24	0.05	0.06	0.12	0.18	0.08	0.08										
SiO_2	0.03	0.00	0.00	0.01	0.00	0.01	0.00	0.01	0.03										
SrO	0.14	0.18	0.16	0.18	0.17	0.11	0.15	0.16	0.16										
CaO	52.41	52.68	52.25	53.20	53.57	53.39	53.36	53.11	53.27										
P_2O_5	42.93	43.08	42.59	41.73	41.84	42.91	42.72	42.79	42.83										
O=F,Cl	−1.36	−1.48	−1.12	−1.29	−1.60	−1.69	−1.37	−0.73	−1.62										
Total	97.92	97.44	97.03	97.07	97.43	98.53	98.12	97.60	98.41										

	Type 1 monazite		Type 2 monazite								
Sample	1	2	1	2	3	4	5	6	7	8	9
F	0.37	0.16	0.18	0.21	0.04	0.28	0.82	0.69	0.22	0.87	0.90
SiO_2	0.03	0.04	0.03	0.03	0.01	0.02	0.20	0.00	0.01	0.03	0.03
CaO	0.10	0.20	0.22	0.22	0.65	0.39	1.11	1.03	0.18	0.66	0.79
P_2O_5	31.11	31.39	30.17	29.54	32.06	28.95	30.50	31.98	30.28	29.94	29.54
ThO_2	0.00	0.13	0.22	0.00	0.00	0.13	0.07	0.06	0.19	0.00	0.28

(*continued on next page*)

Table 2 (*continued*)

UO_2	0.03	0.00		0.00	0.00	0.00	0.00	0.02	0.00	0.01	0.00	0.00
La_2O_3	16.62	16.86		16.56	16.22	18.38	17.43	17.67	16.94	17.09	15.94	16.28
Ce_2O_3	37.96	37.71		37.37	37.63	38.21	39.35	37.04	38.82	40.23	37.74	40.13
Pr_2O_3	3.35	3.35		3.15	3.29	3.07	3.17	3.24	3.28	3.11	3.36	3.46
Nd_2O_3	9.33	9.88		8.66	8.90	8.35	8.72	9.23	8.92	8.55	9.90	8.56
Sm_2O_3	0.82	0.89		1.02	0.90	0.90	0.90	1.11	0.95	0.80	1.21	0.87
Gd_2O_3	0.19	0.17		0.15	0.07	0.08	0.07	0.10	0.13	0.03	0.11	0.13
Dy_2O_3	0.08	0.05		0.00	0.03	0.06	0.00	0.08	0.00	0.05	0.00	0.00
Y_2O_3	0.26	0.51		0.63	0.71	0.51	0.45	0.50	0.26	0.18	0.43	0.24
O=F	−0.16	−0.07		−0.08	−0.09	−0.02	−0.12	−0.35	−0.29	−0.09	−0.37	−0.38
Total	99.92	101.19		98.17	97.57	102.28	99.61	100.99	102.48	100.98	99.44	100.45

	Type 3 monazite					Type 4 monazite					
Sample	1	2	3	4	5	1	2	3	4	5	6
F	0.30	0.50	0.08	0.00	0.33	0.21	0.35	0.49	0.47	0.55	0.68
SiO_2	0.03	0.04	0.00	0.02	0.00	0.06	0.04	0.05	0.02	0.00	0.00
CaO	0.07	0.08	0.06	0.08	0.04	0.06	0.07	0.03	0.08	0.09	0.08
P_2O_5	33.26	28.76	31.43	32.75	31.56	29.86	31.75	31.49	32.16	31.74	31.40
ThO_2	0.29	0.16	0.62	0.22	0.39	0.08	0.03	0.18	0.32	0.30	0.10
UO_2	0.00	0.00	0.00	0.00	0.00	0.00	0.00	0.07	0.00	0.00	0.00
La_2O_3	17.72	17.01	17.35	20.24	15.95	13.25	13.28	13.62	12.26	13.92	13.34
Ce_2O_3	40.59	39.92	39.53	38.88	40.78	40.51	41.21	41.39	38.90	41.36	41.22
Pr_2O_3	3.33	3.23	3.17	2.89	3.39	4.18	4.06	4.00	4.38	3.97	4.42
Nd_2O_3	8.35	8.22	8.48	7.60	8.60	11.34	11.17	11.18	11.71	11.13	11.24
Sm_2O_3	0.75	0.48	0.66	0.52	0.65	0.85	0.73	0.76	0.66	0.70	0.77
Gd_2O_3	0.25	0.19	0.13	0.04	0.07	0.19	0.14	0.01	0.13	0.04	0.18
Dy_2O_3	0.00	0.00	0.00	0.00	0.00	0.04	0.00	0.01	0.02	0.00	0.07
Y_2O_3	0.13	0.07	0.11	0.03	0.08	0.01	0.00	0.10	0.13	0.00	0.01
O=F	−0.13	−0.21	−0.03	0.00	−0.14	−0.09	−0.15	−0.21	−0.20	−0.23	−0.29
Total	104.82	98.24	101.65	103.27	101.56	100.46	102.52	102.95	100.85	103.32	104.82

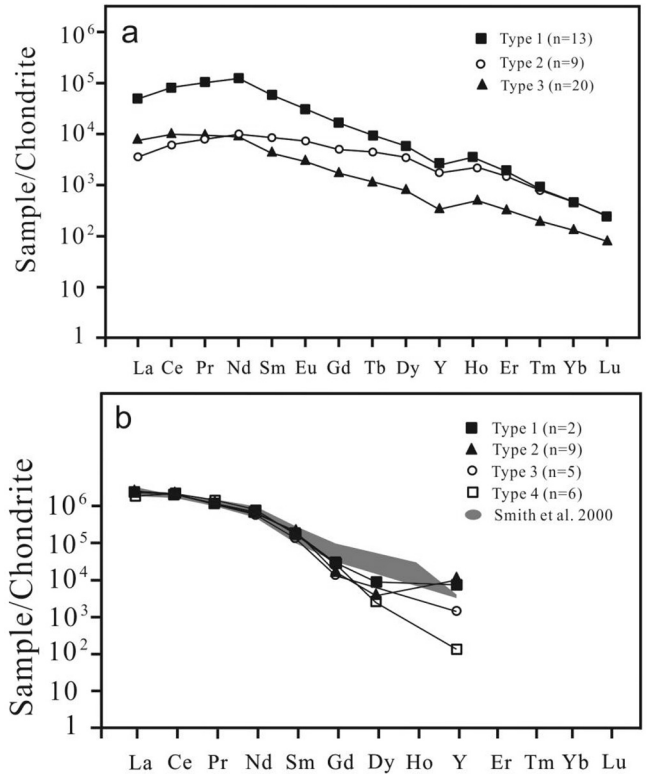

Fig. 5. Chondrite-normalized REE abundance diagrams for three types of apatites (a) and four types of monazites (b) at the Bayan Obo deposit. Normalization values from McDonough and Sun (1995).

aegirine, arfvedsonite, phlogopite, diopside, barite and fluorite, and resulted in the formation of different ore types. Some associated phases such as apatite (Campbell and Henderson, 1997) and metasomatic silicate minerals (Smith, 2007) in the orebody have been studied previously and were considered to be related to either metasomatism, or to post-depositional metamorphism. The combination of fluid flow and metamorphism is responsible for much of the mineralogical complexity of the ores (Smith et al., 2015). However, the nature of metasomatic fluids is not well constrained. Apatite is a widespread accessory mineral in different igneous, metamorphic, and sedimentary rocks. The crystallization of apatite is an important process in geological systems being the host of important trace elements such as REE and Sr, controlled through apatite/melt equilibria (Toplis and Dingwell, 1996). Three types of apatites have been observed in this study, and may record the metasomatic processes and provide important clues as to the fluid composition.

Type 1 apatite occurs as primary grains, and shows high Sr (5461–6892 ppm), REE contents (~6000 ppm La) and strong LREE enrichment [$(La/Yb)_{CN}$ = 30–291] with neglectable Ce and Eu anomalies, clearly distinguishing them from those in mafic rocks, granitoid and granite pegmatites with Sr < 1200 ppm (Belousova et al., 2002) and from sedimentary rocks with lower REE (total REE < 4000 ppm) and LREE fractionation [$(La/Yb)_{CN}$ < 16] and strong Ce and Eu anomalies (Frietsch and Perdahl, 1995; Stalder and Rozendaal, 2004). Belousova et al. (2002) studied trace-element compositions of apatites from different types of rocks, and concluded that the slope of chondrite-normalised REE patterns varies systematically from ultramafic through intermediate to highly fractionated granitoid rock types. Particularly, $(La/Yb)_{CN}$ is very high in apatites from carbonatites, which is similar to our Type 1 apatite. Bühn et al. (2001) found different chemical compositions of apatite during different stages of carbonatite magma evolution that early crystallized apatites have relatively lower REE abundances (La < 1500 ppm), and show convex upward shaped REE pattern with $(La/Nd)_{CN}$ < 1 than that [$(La/Nd)_{CN}$ > 1, and La up to 1 wt%] from fractionated carbonatites. Type 1 apatite also displays LREE depletion relative to MREE, but has higher REE content (La > 6000 ppm) (Fig. 5a) than late-stage ones (Types 2 and 3). This may be explained that REE preferentially partitioned into the monazite and REE-

Table 3
LA-ICPMS analysis of apatites from drill core samples in the Bayan Obo deposit.

	Type 1 apatite												
Sample	1	2	3	4	5	6	7	8	9	10	11	12	13
La	3904	11641	3993	4524	8395	21948	1461	2294	5269	6636	3393	4888	3872
Ce	18019	48690	18140	20744	35173	91245	7091	8640	16628	19147	11625	15961	12865
Pr	3728	9120	3703	4185	6573	16990	1545	1590	2661	2873	2018	2637	2176
Nd	23636	52760	23761	26077	38153	96342	10619	9709	14268	14860	11806	14745	12465
Sm	4132	7682	4247	4441	5664	13006	2185	1869	2267	2221	2092	2389	2167
Eu	898	1497	911	966	1149	2403	515	426	489	479	471	524	482
Gd	1800	2780	1797	1917	2214	4248	1071	929	1036	1007	1010	1095	1028
Tb	206	282	202	222	239	388	130	113	123	119	123	129	124
Dy	910	1123	882	976	1006	1438	601	522	559	550	566	590	580
Y	2518	2799	2338	2630	2613	3276	1751	1614	1733	1698	1779	1784	1798
Ho	128	147	121	136	137	173	86.0	77.4	82.6	81.3	84.3	85.8	86.1
Er	201	225	190	217	215	257	141	132	140	138	146	145	149
Tm	14.4	15.3	13.6	15.6	15.2	16.8	10.1	10.5	11.0	10.8	11.3	11.4	11.4
Yb	49.0	51.3	46.3	53.5	51.5	54.1	34.3	38.4	40.1	39.8	41.1	39.4	43.8
Lu	3.54	3.59	3.33	3.88	3.71	3.61	2.46	2.84	3.00	3.02	3.10	2.94	2.96
Sr	6892	6759	6616	6710	6674	6808	6276	5539	5494	5461	5723	5832	5673
Ba	865	57.6	54.1	80.8	91.1	86.2	98.3	416	84.9	71.5	48.0	301	118
Th	44.3	112	43.9	45.4	85.7	179	16.5	17.6	46.3	61.1	32.4	36.1	48.5
U	–	–	–	0.01	–	0.02	–	0.04	–	–	–	–	–

	Type 2 apatite								
Sample	1	2	3	4	5	6	7	8	9
La	270	206	339	314	646	491	583	708	583
Ce	1522	1250	1679	1441	2693	2150	2415	2928	2422
Pr	390	335	347	281	483	407	427	529	444
Nd	3140	2700	2111	1626	2638	2329	2367	2921	2462
Sm	907	844	680	490	684	661	620	761	652
Eu	236	223	240	166	236	232	212	258	225
Gd	555	530	576	399	562	566	517	620	541
Tb	79.0	76.7	97.4	67.5	91.0	94.3	85.1	99.9	89.8
Dy	409	391	515	361	480	510	451	520	483
Y	1236	1177	1408	1007	1455	1528	1375	1571	1526
Ho	64.8	60.6	79.9	55.7	75.0	79.1	70.5	80.2	77.3
Er	117	107	140	99.0	131	140	124	143	142
Tm	9.55	8.56	11.3	8.16	10.5	11.3	10.5	11.8	12.1
Yb	34.8	30.6	42.0	30.2	43.2	43.4	40.7	47.0	46.8
Lu	2.65	2.22	3.43	2.44	3.33	3.52	3.29	3.94	3.74
Sr	6320	5671	6733	4858	6247	6323	5736	6356	6124
Ba	55.6	78.6	30.8	43.3	38.1	24.5	39.5	35.9	50.2
Th	1.52	0.94	1.47	1.20	2.86	1.64	2.80	3.90	2.22
U	–	0.01	0.03	0.02	–	–	–	–	–

	Type 2 apatite																			
Sample	1	2	3	4	5	6	7	8	9	10	11	12	13	14	15	16	17	18	19	20
La	1005	985	986	1419	1321	1149	1206	1242	1204	708	586	800	1116	1142	1140	715	642	775	447	652
Ce	3253	3312	3182	4628	4334	4043	4558	4665	4258	2483	2057	2789	4191	3876	3907	2372	2142	2586	1566	2176
Pr	462	479	450	637	607	606	709	725	640	382	324	430	653	568	578	363	329	388	259	335
Nd	2076	2186	2030	2680	2591	2684	3233	3279	2837	1766	1504	1993	2969	2489	2533	1683	1555	1768	1281	1562
Sm	336	357	332	382	366	390	480	467	393	271	237	322	465	383	389	278	265	286	223	266
Eu	91.3	96.4	90.7	95.1	92.0	99.8	119	113	97.9	70.2	62.7	84.2	121	102	101	74.5	71.5	76.5	60.9	71.3
Gd	194	204	194	197	191	207	250	230	202	148	133	181	255	218	218	165	159	169	132	157
Tb	24.9	26.5	25.4	24.5	24.1	25.4	29.0	25.8	23.3	18.4	16.9	23.0	31.2	27.2	27.6	21.0	20.4	21.5	16.9	20.2
Dy	117	123	122	116	115	112	128	110	101	85.3	76.2	105	137	125	124	97.1	93.8	98.7	75.0	93.9
Y	305	314	319	302	302	278	302	258	259	215	197	254	335	325	321	256	252	254	218	253
Ho	18.1	18.6	18.9	17.5	17.2	16.3	18.5	15.7	14.6	12.3	11.4	15.5	19.2	18.5	18.4	14.4	13.9	14.7	12.0	14.2
Er	34.1	35.0	35.6	34.2	33.7	30.5	33.9	29.6	26.0	23.6	21.0	28.7	34.8	34.0	32.5	26.5	25.9	27.1	21.3	26.2
Tm	3.13	3.14	3.38	3.39	3.19	2.83	3.38	2.69	2.39	2.04	1.99	2.80	3.00	3.06	2.85	2.33	2.31	2.41	1.94	2.44
Yb	13.3	13.8	15.0	15.2	14.9	12.3	14.5	11.3	10.4	10.7	9.20	12.3	12.6	12.4	12.4	10.2	9.76	10.4	8.18	10.5
Lu	1.21	1.31	1.38	1.36	1.52	1.22	1.43	0.96	0.89	1.02	0.92	1.08	0.97	1.13	0.99	0.96	0.90	0.93	0.67	0.93
Sr	3812	3863	3965	3253	3201	2684	2786	2548	2228	3339	3224	4313	3737	3815	3747	4317	4368	4273	4169	4307
Ba	103	71.9	44.3	82.3	79.2	73.7	232	72.5	49.5	107	77.9	67.4	124	60.0	59.0	56.0	56.0	79.9	70.3	76.1
Th	3.27	3.49	4.42	7.03	7.24	4.44	5.07	4.09	6.08	4.17	5.16	6.81	3.25	4.16	2.70	5.82	5.08	6.20	5.13	6.30
U	–	–	0.02	–	0.24	–	–	0.04	–	0.04	–	–	–	0.02	–	–	–	0.02	–	0.06

– below the defection limits.

fluorocarbonates than the simultaneously crystallized apatite. We, therefore, suggest that the primary Type 1 apatite was of carbonatitic origin. Moreover, the dolomite in the H8 marble also has high Sr contents and LREE enrichment (Table 3), indicating the same genesis (Hornig-Kjarsgaard, 1998; Chakhmouradian et al., 2016). This conclusion is supported by amounts of carbonatite dyke emplacement around the H8 unit (Yang et al., 2011).

Minor monazite (Type 1) was observed to occur along the Type 1 apatite rim. Based on natural (Hansen and Harlov, 2007) and experimental investigations (Harlov et al., 2005), monazite associated with apatite is considered to be a potential tracer of metasomatic processes via hydrothermal fluids (Harlov and Förster, 2003; Harlov et al., 2002, 2005). Type 1 monazite was possibly formed at the expense of apatite as a result of fluid-induced alteration of apatite via coupled dissolution-reprecipitation processes (Harlov and Förster, 2003; Harlov et al., 2005). According to Zirner et al. (2015), whether apatite breaks down to form monazite or remains stable may be influenced by the availability of Na^+ and Si^{4+} ions to maintain a charge balance in the apatite structure. Removal of Na and Si at high REE levels from the system results in a charge imbalance freeing the REE to react with P and to form monazite.

In geochemical systems, the REE and the pseudolanthanide Y occur exclusively in the trivalent oxidation state, and the closest similarity with respect to ionic radius exists between Y and Ho. The Y and Ho can be expected to behave coherently from the same fluid sources. Neither partial melting nor fractional crystallization significantly fractionate Y and Ho (Bau and Dulski, 1995). Thus, Y/Ho and La/Ho ratios can be used in this study to test whether different types of apatites are cogenetic. Three types of apatites show different Y/Ho ratios (20.8–21.1, 19.3–19.7 and 16.9–17.9, respectively) and follow different trends (highly variable La/Ho ratios at very small range of Y/Ho ratios in Type 1 and Type 3, relatively; constant La/Ho ratios in Type 2), indicating that they crystallized from different fluid sources (Fig. 6a). Moreover, Type 3 apatite has lower Y content than both Types 1 and 2 (Fig. 6b). The significant difference in Sr compositions (4858–6733 ppm and 2228–4368 ppm) of Types 2 and 3 apatites also goes against the idea that the apatites crystallized from the same fluid source at different evolved stages, because Sr-rich minerals are not observed in the drill cores. The three types of apatites show different linear relationship between $(Ce/Nd)_{CN}$ and total REE contents (Fig. 6c). The $^{208}Pb/^{232}Th$ dates of monazite in the Bayan Obo deposit ranging from 331 to 758 Ma (Ling et al., 2013) also imply a multistage fluid evolution history. Therefore, the three types of apatites may have crystallized from different fluid sources.

The apatite and monazite textural and compositional variations clearly suggest that the primary REE mineralization related with carbonatite magmatism has been altered, remobilized and redeposited due to the effect of the hydrothermal metasomatism events. The metasomatic fluids may be rich in Sr as indicated by the high Sr composition of three types of the apatites. Many experimental studies (Williams-Jones et al., 2012) and evidences from hydrothermal REE deposits (Chakhmouradian and Wall, 2012; Liu et al., 2015) clearly demonstrated that the REE can be mobilized by hydrothermal fluids. The hydrothermal events at the Bayan Obo deposit probably occurred after 1.3 Ga and during the time of 500–400 Ma according to the above mentioned dating results of REE minerals and sulfides from the orebody (Wang et al., 1994; Liu, 2004; Hu et al., 2009). The origin of the metasomatism has been proposed to be related with granitic fluids (Wang et al., 1994), Caledonian subduction-related fluids (Ling et al., 2013), or carbonatite-derived fluids (Smith, 2007). Granitic fluids can be excluded based on the fact that apatites from granitoids and granitic pegmatites show extremely low Sr contents (less than 100 ppm) and negative Eu anomaly (Belousova et al., 2002), in contrast to Types 2 and 3 apatites observed in this study. Moreover, large volume of granites, distributed in the eastern and southern region of the deposit, were emplaced at 260–280 Ma (Fan et al., 2009; Ling et al., 2014), and

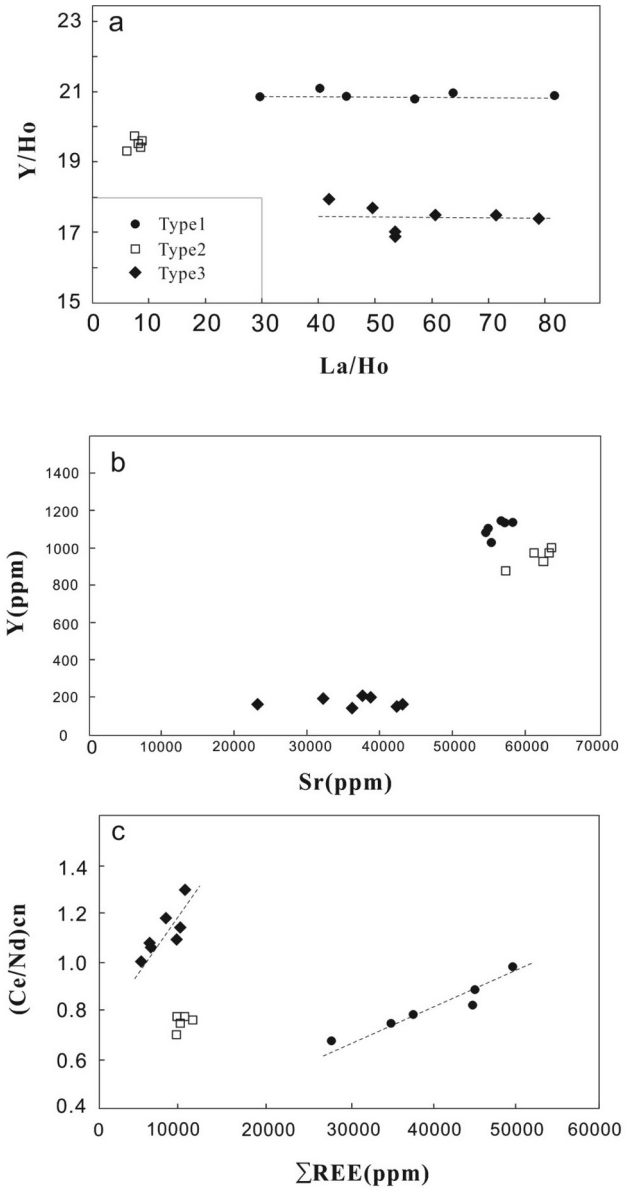

Fig. 6. Y/Ho vs. La/Ho (a), Y vs. Sr (b), and $(Ce/Nd)_{CN}$ vs. total REE (c) diagrams for three types of apatites from the drill cores.

therefore younger than the latest REE mineralization ages. Ling et al. (2013) proposed a model of hydrothermal fluids from subducted slabs scavenging ore-forming metals from inferred deep-seated carbonatites, however there are no Caledonian subduction-related igneous rocks reported in the region (Zhang et al., 2003). Carbonatites, responsible for the primary REE mineralization, are also unlikely to be the metasomatic fluid source due to lack of post-1.3 Ga carbonatite magmatism (Zhang et al., 2003).

The Bayan Obo deposit may not be the result of a single mineralization event, because at least three types of apatites with different textures and chemical compositions have been found in this study (Figs. 5 and 6). The sedimentary rocks at Bayan Obo would be an alternative source for the metasomatic fluids. These rocks experienced greenschist to low amphibolite facies metamorphism due to tectonic deformation (Chao et al., 1997), which also caused the formation of the syncline-shape of the ore-hosting H8 unit, as well as the banding and massive pods of the ores (Smith et al., 2015). During the metamorphic processes, metasomatic fluids derived from the sedimentary rocks may have played a role in remobilization and recrystallization of the primary H8 unit.

6. Conclusions

As distinct from the previously reported REE minerals associated with metasomatic silicates and late-stage fluorite and barite veins in the ore-hosting dolomite marble from Bayan Obo, apatites and monazites in this study have been categorized into three and four types, respectively. These apatites show different texture and REE composition, which indicates that the world-class REE mineralization at Bayan Obo was not a single event. The primary apatites are characterized by high Sr and REE contents, indicating a carbonatitic origin. Multi-stage metasomatism further resulted in remobilization and recrystallization of the original REE minerals. Metasomatic fluids may be derived from the sedimentary rocks at Bayan Obo, which underwent different-degree metamorphism. More isotopic studies are needed to further constrain the source of the metasomatic fluids.

Acknowledgments

We are particularly grateful to Editor Prof. Franco Pirajno and two anonymous reviewers for reviewing and improving the manuscript. This research was financially supported by Chinese National Science Foundation (Nos. 41573033; 41773022) and Chinese '973' Project (No. 2013CB429800).

References

Bai, G., Yuan, Z.X., 1985. Carbonatites and related mineral resources. Bull. Inst. Miner. Deposit. Chin. Acad. Geol. Sci. 13, 107–140.
Bau, M., Dulski, P., 1995. Comparative study of yttrium and rare-earth element behaviors in fluorine-rich hydrothermal fluids. Contrib. Miner. Petrol. 119, 213–223.
Belousova, E.A., Griffin, W.L., O'Reilly, S.Y., Fisher, N.I., 2002. Apatite as an indicator mineral for mineral exploration: trace-element compositions and their relationship to host rock type. J. Geochem. Explor. 76, 45–69.
Bühn, B., Wall, F., Le Bas, M.J., 2001. Rare-earth element systematics of carbonatitic fluorapatites, and their significance for carbonatite magma evolution. Contrib. Miner. Petrol. 141, 572–591.
Campbell, L.S., Henderson, P., 1997. Apatite paragenesis in the Bayan Obo REE-Nb-Fe ore deposit, Inner Mongolia, China. Lithos 42, 89–103.
Chakhmouradian, A.R., Wall, F., 2012. Rare earth elements: minerals, mines, magnets (and more). Elements 8, 333–340.
Chakhmouradian, A.R., Reguir, E.P., Couëslan, C., Yang, P., 2016. Calcite and dolomite in intrusive carbonatites. II. Trace-element variations. Mineral. Petrol. 110, 361–377.
Chao, E.C.T., Back, J.M., Minkin, J.A., Ren, Y., 1992. Host-rock controlled epigenetic, hydrothermal metasomatic origin of the Bayan Obo REE–Fe–Nb ore deposit, Inner Mongolia, P.R.C. Appl. Geochem. 7, 443–458.
Chao, E.C.T., Back, J.M., Minkin, J.A., Ren, Y., 1997. The sedimentary carbonate giant Bayan Obo REE–Fe–Nb ore deposit of Inner Mongolia, China: a cornerstone example for giant polymetallic ore deposit of hydrothermal origin. U.S. Geol. Surv. Bull. 2143, 1–65.
Fan, H.R., Hu, F.F., Yang, K.F., Wang, K.Y., Liu, Y.S., 2009. Geochronology framework of late Paleozoic Dioritic-Gianitic Plutons in the Bayan Obo Area, Inner Mongolia, and tectonic significance. Acta Petrol. Sin. 25, 2933–2938.
Fan, H.R., Hu, F.F., Yang, K.F., Pirajno, F., Liu, X., Wang, K.Y., 2014. Integrated U-Pb and Sm-Nd geochronology for a REE-rich carbonatite dyke at the giant Bayan Obo REE deposit, Northern China. Ore Geol. Rev. 63, 510–519.
Fan, H.-R., Yang, K.-F., Hu, F.-F., Liu, S., Wang, K.-Y., 2016. The giant Bayan Obo REE-Nb-Fe deposit, China: controversy and ore genesis. Geosci. Front. 7, 335–344.
Frietsch, R., Perdahl, J.A., 1995. Rare earth elements in apatite and magnetite in Kiruna-type iron ores and some other iron ore types. Ore Geol. Rev. 9, 489–510.
Geological Survey, U.S., 2017. Mineral Commodity Summaries 2017. U.S. Geological Survey, Washington, U.S.
Hansen, E.C., Harlov, D.E., 2007. Whole-rock, phosphate, and silicate compositional trends across an amphibolite- to granulite-facies transition, Tamil Nadu, India. J. Petrol. 48, 1641–1680.
Harlov, D.E., Förster, H.J., 2003. Fluid-induced nucleation of (Y + REE)-phosphate minerals within apatite: Nature and experiment. Part II. Fluorapatite. Am. Mineral. 88, 1209–1229.
Harlov, D.E., Förster, H.J., Nijland, T.G., 2002. Fluid-induced nucleation of (Y + REE)-phosphate minerals within apatite: Nature and experiment. Part I. Chlorapatite. Am. Mineral. 87, 245–261.
Harlov, D.E., Wirth, R., Förster, H.J., 2005. An experimental study of dissolution–reprecipitation in fluorapatite: fluid infiltration and the formation of monazite. Contrib. Miner. Petrol. 150, 268–286.
Hornig-Kjarsgaard, I., 1998. Rare earth elements in sovitic carbonatites and their mineral phases. J. Petrol. 39, 2105–2121.
Hu, F.-F., Fan, H.-R., Liu, S., Yang, K.-F., Chen, F., 2009. Samarium-neodymium and rubidium-strontium isotopic dating of veined REE mineralization for the Bayan Obo REE-Nb-Fe deposit, Northern China. Resour. Geol. 59, 407–414.
Institute of Geochemistry, Chinese Academy of Sciences, 1988. The Geochemical Composition and Mineralization Regularity of Bayan Obo Deposit, Inner Mongolia. Science Press, Beijing.
Le Bas, M.J., Keller, J., Tao, K.-J., Wall, F., Williams, C.T., Zhang, P.-S., 1992. Carbonatite dykes at Bayan Obo, Inner Mongolia, China. Mineral. Petrol. 72, 195–228.
Ling, M.-X., Liu, Y.-L., Williams, I.S., Teng, F.-Z., Yang, X.-Y., Ding, X., Wei, G.-J., Xie, L.-H., Deng, W.-F., Sun, W.-D., 2013. Formation of the world's largest REE deposit through protracted fluxing of carbonatite by subduction-derived fluids. Sci. Rep. 3, 1776.
Liu, Y., 2004. Re-Os dating of pyrite from Giant Bayan Obo REE-Nb-Fe deposit. Chin. Sci. Bull. 49, 2627.
Liu, Y., Hou, Z., 2017. A synthesis of mineralization styles with an integrated genetic model of carbonatite-syenite-hosted REE deposits in the Cenozoic Mianning-Dechang REE metallogenic belt, the eastern Tibetan Plateau, southwestern China. J. Asian Earth Sci. 137, 35–79.
Liu, Y., Zhu, Z., Chen, C., Zhang, S., Sun, X., Yang, Z., Liang, W., 2015. Geochemical and mineralogical characteristics of weathered ore in the Dalucao REE deposit, Mianning–Dechang REE Belt, western Sichuan Province, Southwestern China. Ore Geol. Rev. 71, 437–456.
McDonough, W.F., Sun, S.-S., 1995. The composition of the Earth. Chem. Geol. 120, 223–253.
Meng, Q.-R., 1982. The genesis of the host rock dolomite of the Bayan Obo iron ore deposit and analysis of its sedimentary environment. Geol. Rev. 28, 481–489 (in Chinese with English abstract).
Smith, M.P., 2007. Metasomatic silicate chemistry at the Bayan Obo Fe–REE–Nb deposit, Inner Mongolia, China: contrasting chemistry and evolution of fenitising and mineralising fluids. Lithos 93, 126–148.
Smith, M.P., Henderson, P., Zhang, P.-S., 1999. Reaction relationships in the Bayan Obo Fe-REE-Nb deposit Inner Mongolia, China: implications for the relative stability of rare-earth element phosphates and fluorocarbonates. Contrib. Miner. Petrol. 134, 294–310.
Smith, M.P., Henderson, P., Campbell, L., 2000. Fractionation of the REE during hydrothermal processes: constraints from the Bayan Obo Fe-REE-Nb deposit, Inner Mongolia, China. Geochim. Cosmochim. Acta 64, 3141–3160.
Smith, M.P., Campbell, L., Kynicky, J., 2015. A review of the genesis of the world class Bayan Obo Fe–REE–Nb deposits, Inner Mongolia, China: Multistage processes and outstanding questions. Ore Geol. Rev. 64, 459–476.
Stalder, M., Rozendaal, A., 2004. Apatite nodules as an indicator of depositional environment and ore genesis for the Mesoproterozoic Broken Hill-type Gamsberg Zn–Pb deposit, Namaqua Province, South Africa. Miner. Deposita 39, 189–203.
Toplis, M.J., Dingwell, D.B., 1996. The variable influence of P_2O_5 on the viscosity of melts of differing alkali/aluminium ratio: Implications for the structural role of phosphorus in silicate melts. Geochim. Cosmochim. Acta 60, 4107–4121.
Wang, J., Tatsumoto, M., Li, X., Premo, W.-R., Chao, E.T.C., 1994. A precise 232Th-208Pb chronology of fine-grained monazite: age of the Bayan Obo REE-Fe-Nb ore deposit, China. Geochim. Cosmochim. Acta 58, 3155–3169.
Xie, Y., Hou, Z., Goldfarb, R.J., Guo, X., Wang, L., 2016. Rare earth element deposits in China. Econ. Geol. 18, 115–136.
Xu, C., Campbell, I.H., Kynicky, J., Allen, C.M., Chen, Y., Huang, Z., Qi, L., 2008. Comparison of the Daluxiang and Maoniuping carbonatitic REE deposits with Bayan Obo REE deposit, China. Lithos 106, 12–24.
Xu, C., Taylor, R.N., Li, W., Kynicky, J., Chakhmouradian, A.R., Song, W.-L., 2012. Comparison of fluorite geochemistry from REE deposits in the Panxi region and Bayan Obo, China. J. Asian Earth Sci. 57, 76–89.
Yang, X.-M., Le Bas, M.J., 2004. Chemical compositions of carbonate minerals from Bayan Obo, Inner Mongolia, China: implications for petrogenesis. Lithos 72, 97–116.
Yang, X.-Y., Sun, W.-D., Zhang, Y.-X., Zheng, Y.-F., 2009. Geochemical constraints on the genesis of the Bayan Obo Fe–Nb–REE deposit in Inner Mongolia, China. Geochim. Cosmochim. Acta 73, 1417–1435.
Yang, K.-F., Fan, H.-R., Santosh, M., Hu, F.-F., Wang, K.-Y., 2011. Mesoproterozoic carbonatitic magmatism in the Bayan Obo deposit, Inner Mongolia, North China: constraints for the mechanism of super accumulation of rare earth elements. Ore Geol. Rev. 40, 122–131.
Yang, X.-Y., Lai, X.-D., Franco, P., Liu, Y.-L., Ling, M.-X., Sun, W.-D., 2017. Genesis of the Bayan Obo Fe-REE-Nb formation in Inner Mongolia, north China craton: a perspective review. Precambr. Res. 288, 39–71.
Zhang, Z.Q., Yuan, Z.X., Tang, S.H., Bai, G., Wang, J.H., 2003. Age and Geochemistry of the Bayan Obo Ore Deposit. Geological Publishing House, Beijing.
Zhang, S.H., Zhao, Y., Li, Q.L., Hu, Z.C., Chen, Z.Y., 2017. First identification of baddeleyite related/linked to contact metamorphism from carbonatites in the world's largest REE deposit, Bayan Obo in North China Craton. Lithos 284–285, 654–665.
Zhao, G., Sun, M., Wilde, S.A., Li, S., 2003. Assembly, accretion and breakup of the Paleo-Mesoproterozoic Columbia supercontinent: records in the North China Craton. Gondwana Res. 6, 417–434.
Zirner, A.L.K., Marks, M.A.W., Wenzel, T., Jacob, D.E., Markl, G., 2015. Rare earth elements in apatite as a monitor of magmatic and metasomatic processes: the Ilimaussaq complex, South Greenland. Lithos 228, 12–22.